

# Dynamics in next-generation solar cells: time-resolved surface photovoltage measurements of quantum dots chemically linked to ZnO (1010)

Ben F. Spencer,<sup>\*ab</sup> Matthew J. Cliffe,<sup>ab</sup> Darren M. Graham,<sup>a</sup> Samantha J. O. Hardman,<sup>c</sup> Elaine A. Seddon,<sup>ab</sup> Karen L. Syres,<sup>d</sup> Andrew G. Thomas,<sup>a</sup> Fausto Sirotti,<sup>e</sup> Mathieu G. Silly,<sup>e</sup> Javeed Akhtar,<sup>fg</sup> Paul O'Brien,<sup>f</sup> Simon M. Fairclough,<sup>h</sup> Jason M. Smith,<sup>i</sup> Swapan Chattopadhyay<sup>b</sup> and Wendy R. Flavell<sup>a</sup>

Received 21st February 2014, Accepted 11th March 2014

DOI: 10.1039/c4fd00019f

The charge dynamics at the surface of the transparent conducting oxide and photoanode material ZnO are investigated in the presence and absence of light-harvesting colloidal quantum dots (QDs). The time-resolved change in surface potential upon photoexcitation has been measured in the *m*-plane ZnO (1010) using a laser pump-synchrotron X-ray probe methodology. By varying the oxygen annealing conditions, and hence the oxygen vacancy concentration of the sample, we find that dark carrier lifetimes at the ZnO surface vary from hundreds of  $\mu\text{s}$  to ms timescales, *i.e.* a persistent photoconductivity (PPC) is observed. The highly-controlled nature of our experiments under ultra-high vacuum (UHV), and the use of band-gap and sub-band-gap photoexcitation, allow us to demonstrate that defect states *ca.* 340 meV above the valence band edge are directly associated with the PPC, and that the PPC mediated by these defects dominates over the oxygen photodesorption mechanism. These observations are consistent with the hypothesis that ionized oxygen vacancy states are

<sup>a</sup>School of Physics and Astronomy and the Photon Science Institute, The University of Manchester, Manchester M13 9PL, United Kingdom. E-mail: ben.spencer@manchester.ac.uk

<sup>b</sup>The Cockcroft Institute, Sci-Tech Daresbury, Keckwick Lane, Daresbury, Warrington WA4 4AD, Cheshire, United Kingdom

<sup>c</sup>Manchester Institute of Biotechnology, Faculty of Life Sciences, University of Manchester, 131 Princess Street, Manchester M1 7DN, United Kingdom

<sup>d</sup>School of Chemistry, The University of Nottingham, University Park, Nottingham NG7 2RD, United Kingdom

<sup>e</sup>Synchrotron SOLEIL, BP 48, Saint-Aubin, F91192 Gif sur Yvette CEDEX, France

<sup>f</sup>Department of Chemistry, University of Manchester, Oxford Road, Manchester M13 9PL, United Kingdom

<sup>g</sup>Department of Physics, Nano-Science & Materials Synthesis Laboratory, COMSATS Institute of Information Technology, Chakshahzad Park Road, Islamabad 44000, Pakistan

<sup>h</sup>Department of Chemistry, University of Oxford, South Parks Road, Oxford OX1 3QR, United Kingdom

<sup>i</sup>Department of Materials, University of Oxford, Parks Road, Oxford OX1 3PH, United Kingdom



responsible for the PPC in ZnO. The effect of chemically linking two colloidal QD systems (type I PbS and type II CdS–ZnSe) to the surface has also been investigated. Upon deposition of the QDs onto the surface, the dark carrier lifetime and the surface photovoltage are reduced, suggesting a direct injection of charge carriers into the ZnO conduction band. The results are discussed in the context of the development of next-generation solar cells.

## Introduction

The urgent need to reduce the cost of solar energy technology has led to an increasing interest in the transparent conducting oxide (TCO) ZnO as a potential photoanode,<sup>1–3</sup> particularly as part of next-generation solar cells utilising colloidal quantum dots (QDs) as the light harvesters.<sup>4–6</sup>

ZnO exhibits a persistent photoconductivity (PPC) after the excitation source has been switched off which, along with its large band gap of  $\sim 3.4$  eV,<sup>1,2,7</sup> makes it ideal as a photoanode material.<sup>1</sup> However, the origin of this PPC has been controversial:<sup>1</sup> for some years the capture of holes by chemisorbed oxygen was thought to be the primary mechanism,<sup>8–14</sup> and the surrounding oxygen environment has also been shown to influence the lifetime of PPC.<sup>15,16</sup> More recent theoretical work has instead suggested that oxygen vacancies play an important part in the PPC mechanism because band-gap states associated with metastable doubly-<sup>17–19</sup> or singly-charged<sup>20</sup> oxygen vacancies control the PPC, and recent experimental work has now strengthened this hypothesis.<sup>21,22</sup>

Colloidal QDs are nanometre-sized semiconductor crystals with sizes comparable to the Bohr radius of an exciton in the corresponding bulk material. This quantum confinement means that the effective band gap is tuned with the size of the nanocrystal.<sup>23,24</sup> QDs may also be especially useful for photovoltaic applications since many studies have shown that multiple carriers can be generated with increased efficiency over bulk materials by a single photon that is in excess of the band gap because the excess energy loss by phonon absorption is reduced; instead this excess energy creates additional carriers.<sup>25–27</sup> These quantum effects allow for the theoretical maximum efficiency of single junction solar cells (the Shockley–Queisser limit of approximately 30%)<sup>28</sup> to be overcome. Carrier multiplication has been identified in many QD materials including PbS,<sup>5</sup> PbSe,<sup>26</sup> InP,<sup>29</sup> InAs,<sup>30</sup> CdSe,<sup>31</sup> CdTe<sup>32</sup> and Si.<sup>33</sup> Photovoltaic devices using PbS QDs with carrier multiplication have already been implemented.<sup>34</sup>

A 'core–shell' structure may be introduced to passivate the QD or to engineer its electronic structure. So-called 'type I' QDs are those where on photoexcitation, the electrons and holes are both confined to either the core or shell of the nanocrystal. More recently, type II core–shell structures, which have a staggered band alignment, have become of greater interest because the photogenerated electron and hole can be separately localized in the core and shell of the QD, or *vice versa*. The core and shell thicknesses can effectively control the electron and hole wavefunction overlap and hence the recombination lifetime.<sup>35–37</sup> Type II core–shell QD structures studied so far include CdS–ZnSe,<sup>35</sup> CdSe–ZnTe,<sup>38</sup> CdTe–CdS,<sup>39</sup> CdTe–ZnTe,<sup>40</sup> CdTe–CdSe<sup>41</sup> and ZnTe–ZnSe.<sup>42,43</sup>

A proposed model for a next-generation solar cell includes the use of colloidal QDs as light harvesters and ZnO as the photoanode. Clearly the charge carrier



dynamics at the interface must be well understood in order for such a solar cell to be designed. These may be probed through the surface potential change upon photoexcitation in the ZnO substrate. Upon photoexcitation, in the presence of a surface depletion layer (for an  $n$ -type semiconductor), electrons are promoted into the conduction band and migrate into the bulk, reducing the amount of band bending at the surface (Fig. 1). This change in the surface potential upon photoexcitation is known as the surface photovoltage (SPV) effect.<sup>44,45</sup> This effect can be observed using photoemission spectroscopy, or by illuminating the surface with laser radiation of energy larger than the band gap. Photoexcitation using a pulsed laser then allows for the time-dependent SPV to be probed using X-ray photoelectron spectroscopy (XPS).<sup>21</sup>

SPV measurements have been made on a variety of materials using both optical<sup>46–56</sup> and free-electron laser (FEL) pump beams<sup>57,58</sup> and a variety of experimental techniques, as recently reviewed by Yamamoto and Matsuda.<sup>59</sup> For example, Widdra *et al.*<sup>50</sup> and Bröcker *et al.*<sup>51</sup> utilized the BESSY synchrotron in single-bunch mode to provide a time window of 800 ns to study the SiO<sub>2</sub>-Si (100) interface; a similar methodology was employed in measurements by us at the UK Synchrotron Radiation Source (SRS) in single-bunch mode to study the Si (111)  $7 \times 7$  surface over a 320 ns time window.<sup>21</sup>

The PPC displayed by ZnO requires the use of transient SPV measurements on much longer timescales ( $\mu$ s to seconds). For these measurements we have used a modulated continuous-wave laser in conjunction with ns XPS at Synchrotron SOLEIL. The time period of the experiment is set by a signal generator that

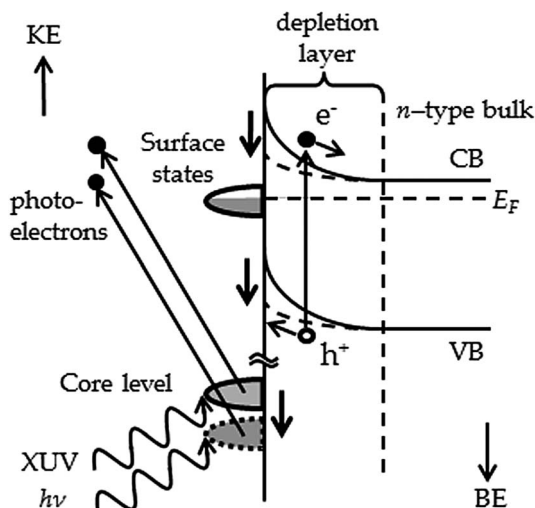


Fig. 1 Non-equilibrium SPV in a conventional  $n$ -type semiconductor. Laser illumination promotes electrons ( $e^-$ ) across the band gap from the valence band (VB) to the conduction band (CB), which then migrate into the bulk due to the presence of a depletion layer. The corresponding holes ( $h^+$ ) migrate to the surface. The electric field within the space charge region and hence the band bending are reduced (dashed lines). The binding energy (BE) of the core electron energy levels are thus increased, reducing the kinetic energy (KE) of the photoelectrons liberated upon X-ray absorption. Here,  $E_F$  denotes the Fermi level prior to photoexcitation, which is pinned by the surface states.



modulates the laser and triggers the XPS measurements, as detailed below. We study the effect of varying the oxygen vacancy content in the *m*-plane ZnO upon the transient SPV using band gap and sub-band gap laser radiation which demonstrates that sub-band gap states associated with oxygen vacancies are responsible for the PPC in ZnO. We show a consistent decrease in the SPV lifetimes upon photoexcitation when type I PbS QDs or type II CdS–ZnSe QDs are chemically linked to the ZnO substrate using 3-MPA ligands. The increase in lifetimes suggests that the attached QDs allow for direct injection of carriers into the conduction band of ZnO. Given the PPC in ZnO is controlled by oxygen vacancy concentration (*i.e.* sample preparation) this indicates that a QD–ZnO system could be a suitable basis for next-generation photovoltaics.

## SPV theory

The amount of band bending at a semiconductor surface changes under photoexcitation. The total change in the band bending at the surface, or surface photovoltage  $\Delta V_{SP}^{tot}$ , upon illumination is described by:<sup>60</sup>

$$\frac{\Delta V_{SP}^{tot}}{kT} \exp\left(\frac{\Delta V_{SP}^{tot}}{kT}\right) = \frac{n_p}{n_0} \exp\left(\frac{V_0}{kT}\right). \quad (1)$$

Here,  $n_0$  is the doping carrier concentration,  $n_p$  is the photoexcited carrier concentration and  $V_0$  is the equilibrium band bending. In our experiment, where we measure the change in SPV,  $\Delta V_{SP}$ , induced by the laser illumination, the photoexcited carrier concentration is determined using the laser fluence, energy and absorption coefficient. A change in the surface potential also affects the photoexcited carrier lifetime,  $\tau$ ,<sup>50</sup>

$$\tau = \tau_\infty \exp\left(\frac{-\Delta V_{SP}}{\alpha kT}\right) \quad (2)$$

where  $\alpha$  is a material parameter (typically with values ranging from 0.5 to 2)<sup>51</sup> and  $\tau_\infty$  is the dark carrier lifetime (the lifetime of carriers in the absence of a surface photovoltage). The parameter  $\alpha$  is likened to the ideality factor in a Schottky diode.<sup>44</sup> A theoretical study by Schulz *et al.* on *p*-type silicon (with a doping level of  $10^{15} \text{ cm}^{-3}$ ) showed that values for  $\alpha$  were consistently less than 1, and that the parameter also correlated with the equilibrium band bending  $V_0$ .<sup>61</sup>

After photoexcitation, the recombination rate is assumed to be limited by the process of overcoming the barrier induced by the band bending by thermionic emission across the depletion layer.<sup>50</sup> The SPV shift reduces in a dynamic way as recombination occurs (eqn (1)), and thus the photoexcited carrier lifetime increases with time (eqn (2)) as the surface potential returns to equilibrium. The decay of the SPV after the laser is switched off is thus modelled as a constant deceleration, as developed in Widdra *et al.*<sup>50</sup> and Bröcker *et al.*<sup>51</sup> For the  $\Delta V_{SP}^{tot} > kT$  case, the decay of the SPV shift over time,  $\Delta V_{SP}(t)$ , can be described by:<sup>50</sup>

$$\Delta V_{SP}(t) = -\alpha kT \ln\left(\exp\left(\frac{-\Delta V_{SP}^{tot}}{\alpha kT}\right) + \frac{t}{\tau_\infty}\right). \quad (3)$$

For the case where  $\Delta V_{SP}^{tot} \sim kT$ , a more general form has been proposed:<sup>51</sup>



$$\Delta V_{SP}(t) = -\alpha kT \ln \left[ 1 - \exp\left(\frac{-t}{\tau_{\infty}}\right) \left( 1 - \exp\left(\frac{-\Delta V_{SP}^{tot}}{\alpha kT}\right) \right) \right]. \quad (4)$$

The onset of the pump-induced SPV change when the laser is switched on may be modelled by a single exponential if the rate of carrier creation far exceeds recombination (*i.e.* at sufficiently high fluence).<sup>44</sup> Otherwise, a bi-exponential or a ‘decelerated’ exponential model analogous to eqn (4) may be appropriate. The latter reflects the dynamic increase in recombination rate as the surface band bending is reduced, which acts to counterbalance the rate of carrier creation.

In this model, the pump-induced change in the surface band bending is logarithmically dependent on the number of induced charge carriers (eqn (1)) and hence the photoexcitation fluence,  $\Phi$ ,

$$\Delta V_{SP}^{tot}(\Phi) = \alpha kT \ln(1 + \gamma \Phi), \quad (5)$$

where  $\gamma$  is another material parameter.<sup>51</sup>

## Experimental

Time-resolved laser pump-synchrotron XPS probe experiments were carried out using a laser in combination with the TEMPO beamline at Synchrotron SOL-EIL.<sup>21,62</sup> A 10 mW CW laser (Coherent, CUBE) operating at 372 nm (3.33 eV) was modulated using a square-wave signal from a pulse generator, typically switching the laser on every 0.5 ms (*i.e.* a repetition rate of 2 kHz) to 2 ms (500 Hz), giving a fluence of approximately 25  $\mu\text{J cm}^{-2}$ . The pulse generator was also used to simultaneously trigger in-house software recording a narrow BE-range XPS spectrum (with a  $\sim 2$  eV window) every 50 ns. These spectra were recorded using a SCIENTA SES 2002 analyser with a two-dimensional (2D) delay-line detector.<sup>63,64</sup> The time resolution was determined to be approximately 150 ns, which was



Fig. 2 Image of the laser beam overlapping the X-ray probe beam on the ZnO sample (measuring 5 × 10 mm) taken using a CCD camera at the TEMPO beamline, SOLEIL.



limited by the time difference in the signals from the delay-line detector and the speed of the electronics. Data were recorded over the time period of the pulse generator, which had a 50% duty cycle meaning the laser was illuminating the sample for half of the time period. In excess of 10 000 accumulations were required to achieve satisfactory signal-to-noise ratios. Spatial overlap of the X-ray probe beam (measuring 150  $\mu\text{m}$  vertically by 100  $\mu\text{m}$  horizontally) with the laser pump beam was achieved using a charge-coupled device (CCD) camera (Fig. 2). A photon energy of 200 eV was used to examine the Zn 3d core level, and the typical experimental resolution was 150 meV (monochromator + analyser). Care was taken to check for and eliminate sample charging: static measurements with and without laser illumination were measured repetitively to ensure that the spectrum returned exactly to its original BE position once illumination had stopped before transient measurements were started.

## Materials

### ZnO preparation

The *m*-plane ZnO (10 $\bar{1}$ 0) surface was prepared using an established recipe.<sup>65–69</sup> The surface *n*-type conductivity of ZnO may be enhanced in UHV by sputtering, a process that creates donors such as oxygen vacancies at the surface<sup>70–72</sup> (possibly together with other defects and defect complexes with oxygen vacancies).<sup>1,2,66</sup> Careful sample preparation is required to enhance the surface concentration of these vacancies in order to avoid sample charging in photoemission. The sample underwent three cycles of argon ion sputtering and electron beam annealing, up to a temperature of 1023–1043 K. Following this, the sample was then annealed in 1.2–1.4  $\times 10^{-7}$  mbar oxygen at 703 K in order to heal some of the excess oxygen vacancies created by sputtering at the surface.<sup>66</sup> This step is important in controlling the final conductivity of the surface. In order to explore the effect of the oxygen vacancy concentration on the dynamics, the annealing period was varied between 10 and 20 min, creating different oxygen vacancy (and hence donor) concentrations in the near-surface layers.<sup>73–75</sup> The sample was then allowed to cool in the presence of oxygen, before a low temperature anneal (603 K, 20 min), followed by a short high temperature anneal *in vacuo* (1023–1043 K, 10 min),<sup>76</sup> completing the cleaning process. A final high temperature flash anneal *in vacuo* has previously been used to remove residual adsorbed oxygen;<sup>76</sup> here it was found to be necessary to eliminate charging during the pump–probe experiment.

The surface was diagnosed as uncontaminated using low energy electron diffraction, where a sharp ZnO (10 $\bar{1}$ 0) 1  $\times$  1 pattern was obtained,<sup>68</sup> and XPS showing no C 1s signal. Measurements were carried out at room temperature under UHV at pressures in the 1–2  $\times 10^{-10}$  mbar range.

### Colloidal QD samples

The preparation and characterisation of the colloidal type I PbS QD sample has been described previously.<sup>5,6</sup> Briefly, the QDs were prepared using a novel environmentally-benign method that employed olive oil as both the solvent and capping agent.<sup>6</sup> The long-chain olive oil capping groups were found to be highly insulating, and so these were exchanged for 3-mercaptopropionic acid (3-MPA) ligands, which resulted in samples free from charging effects during



photoemission measurements, indicating that charge transport into and out of the QDs was possible.<sup>5</sup> The QDs were characterised as having a mean diameter of 4.6 nm determined from a 1S absorption feature at 1.0 eV,<sup>5,77</sup> with well-defined excitonic features in the absorption spectrum which indicates a relatively small size dispersion.<sup>5</sup> These PbS QDs were also shown to exhibit a carrier multiplication for photon energies above  $\sim 2.5$  times the effective (and tunable) band gap energy (*ca.* 1.0 eV here).<sup>5</sup> These measurements used a home-built transient absorption spectrometer described previously.<sup>29</sup>

The CdS core of the type II core–shell CdS–ZnSe QD sample was synthesized using a modified route previously used for synthesis of CdSe QDs where oleylamine was used as the sole surfactant.<sup>78</sup> The shelling technique used was that detailed by Blackman *et al.*;<sup>79</sup> precursors were injected into the CdS core solution under nitrogen (first the Zn precursor at 523 K, followed by the Se precursor five minutes later) before the temperature was raised to 553 K for twenty minutes.<sup>79</sup> Absorption and photoluminescence (PL) measurements showed a red shift in the first excitonic peak of 130 nm compared to the 5.1 nm diameter CdS core-only QDs (a PL peak shift from 470 to 600 nm as shown in Fig. 3). PL lifetime measurements (Fig. 4) confirm the type II behaviour of this sample, where electrons and holes are confined to the core and shell, respectively (unless photon energies greater than the shell effective band gap are used). The lifetime is fitted with a tri-exponential decay with the longest component at over 70 ns, indicating a type II structure with a significant reduction in the electron and hole wavefunction overlap caused by spatial separation.<sup>37,42,80,81</sup> PL lifetimes are consistently longer in type II than in type I QDs, for example, Kim *et al.* showed that PL lifetimes increased from 9.6 ns for CdTe QDs to 57 ns once a CdSe shell was added.<sup>37</sup> Type I CdS and CdSe QDs typically have PL lifetimes of  $\sim 10$  ns.<sup>82,83</sup> Finally, transmission electron microscopy (TEM) images (Fig. 5) show peanut-shaped

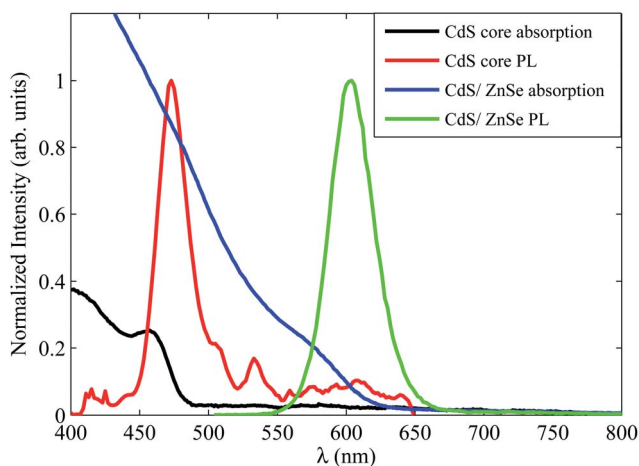


Fig. 3 Absorption and photoluminescence (PL) spectra for CdS core-only QDs and for CdS–ZnSe core–shell QDs, showing a red shift of the PL peak from 470 to 600 nm. The increased width (and the associated spreading seen in the absorption spectra) indicates an increase in size dispersion for the CdS–ZnSe QDs compared to the core-only CdS QDs.



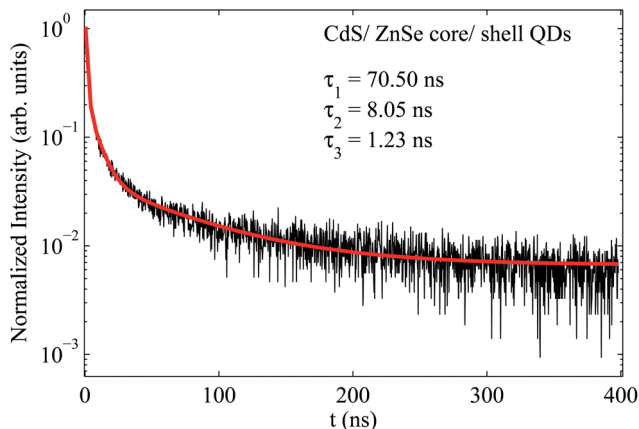


Fig. 4 PL lifetime of the CdS–ZnSe QDs which is fitted with a tri-exponential fit with lifetimes of 70.50, 8.05 and 1.23 ns.

CdS–ZnSe QDs of approximately 6.4 nm width and 8.4 nm in length with a size dispersion of  $\sim 9\%$ .

Ligand exchange between oleylamine and 3-MPA was carried out using the methodology by Aldana *et al.*<sup>84</sup> and the samples were held in solution in chloroform. The QDs were deposited from solution onto the ZnO held *ex situ* outside the UHV chamber for less than one minute to minimize contamination,<sup>5</sup> and the substrate was washed with solvent to remove any QDs not chemically linked to the surface. The presence of the dots attached to the substrate was verified with XPS.

Once chemically attached to ZnO, the energy-level line-up is such that the lowest unoccupied molecular orbital (LUMO) of the QD lies at higher energy than

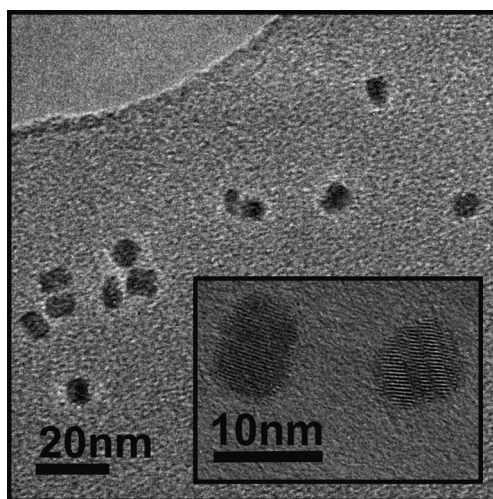


Fig. 5 Low and high (inset) resolution TEM image of the CdS–ZnSe core–shell QDs, showing peanut-shaped QDs with 6.4 nm width and 8.4 nm length with a size dispersion of approximately 9%.



the conduction band minimum in ZnO,<sup>5,6,85,86</sup> and carriers created in the PbS QD or in the shell of the CdS–ZnSe QD (promoted from the highest occupied molecular orbital, or HOMO) may be directly injected into the ZnO CB as shown in Fig. 6. The alignment obtained for the CdS–ZnSe QDs uses the work of Wang *et al.*,<sup>85</sup> Klimov *et al.*,<sup>35</sup> Ivanov and Achermann<sup>86</sup> and the absorption spectrum obtained for the sample (Fig. 3).

## Results

### ZnO (10 $\bar{1}0$ ) with varied oxygen vacancy concentrations

A previous study of the ZnO (10 $\bar{1}0$ ) surface at the SRS, Daresbury Laboratory, indicated no transient change in the SPV upon illumination over the 320 ns time window of these experiments, but a constant SPV shift of 115 meV at all pump–probe delay times, indicating PPC.<sup>21</sup> In order to study longer SPV decay times, we have used the time-resolved XPS facilities at the TEMPO beamline at SOLEIL. Fig. 7 shows XPS of the Zn 3d core level with and without 372 nm laser

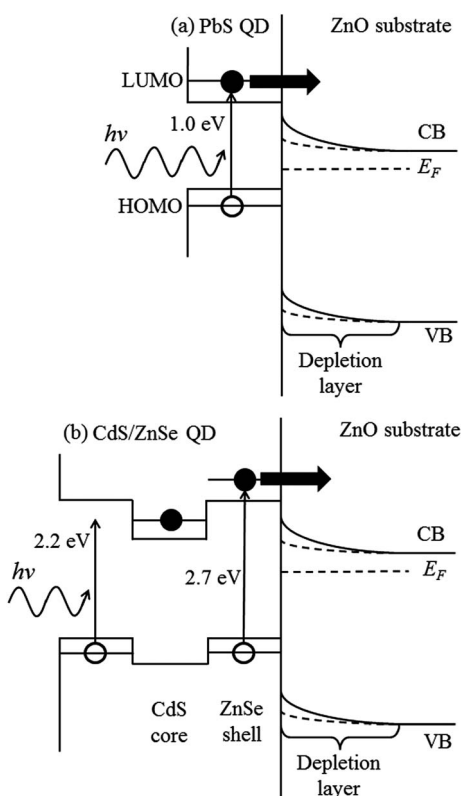


Fig. 6 Schematic energy-level line-up diagrams for (a) PbS QDs and (b) CdS–ZnSe QDs chemically linked to ZnO. The effective band gap energies were determined from the 1S absorption feature in the absorption spectra. In the CdS–ZnSe QD, for photon energies less than 2.7 eV, the type II structure of the QD will trap electrons (filled circles) in the core and holes (open circles) in the shell. For photon energies greater than 2.7 eV electrons in the shell may be photoexcited into the ZnSe CB and injected into the ZnO CB.



illumination; the second 'laser off' spectrum overlies the first, meaning the SPV shift was exactly removed in the absence of laser photoexcitation. The semicore Zn 3*d* level has a complex peak shape influenced by interactions with VB states<sup>87</sup> and is consistent with previous studies of this surface.<sup>88</sup>

In order to probe the PPC of the ZnO surface, time-resolved XPS measurements of the SPV decay following photoexcitation were carried out. The time-dependence of the laser-induced Zn 3*d* core level shift is shown in Fig. 8. As oxygen vacancies have been implicated in the PPC of ZnO,<sup>19,20,89–91</sup> the influence of a change in the concentration of oxygen vacancies (and hence donors), achieved by altering the length of the oxygen annealing cycle, was investigated. Fig. 8 shows the effect of changing the length of this part of the annealing cycle from 20 min to 10 min (Fig. 8(a) and 8(b), respectively). All other experimental conditions are identical. For the 20 min oxygen anneal case, the binding energy of the Zn 3*d* peak is plotted as the laser is switched on at 0 ms, and off after 0.5 ms (shown in the magnified section of Fig. 8(a)). When the laser is switched on, a total core-level shift of 48 meV to a higher binding energy is observed, but the rise time of the shift is very long. The SPV shift reaches its maximum value after approximately 0.1 ms. When the laser is switched off, the SPV shift decays back to equilibrium slowly, over almost half a millisecond.

We use self-decelerating relaxation models to obtain characteristic lifetimes for both the SPV onset and its decay. Eqn (4), rather than eqn (3), was found to provide the best fit of the decay of the pump-induced SPV. This is because in this experiment, the total SPV shift of 48 meV is comparable to  $kT$  ( $\sim 26$  meV), requiring use of the more general form of the expression for the SPV shift (in place of eqn (3)). Likewise, a decelerating exponential increase, analogous to eqn (4), fitted the onset of the SPV shift well. A dark carrier lifetime,  $\tau_{\infty}$ , of 150  $\mu$ s is found for the 20 min oxygen anneal case (Fig. 8(a)). A much larger time constant for the SPV shift of 1.2 ms is found when the oxygen annealing time is reduced (Fig. 8(b)).

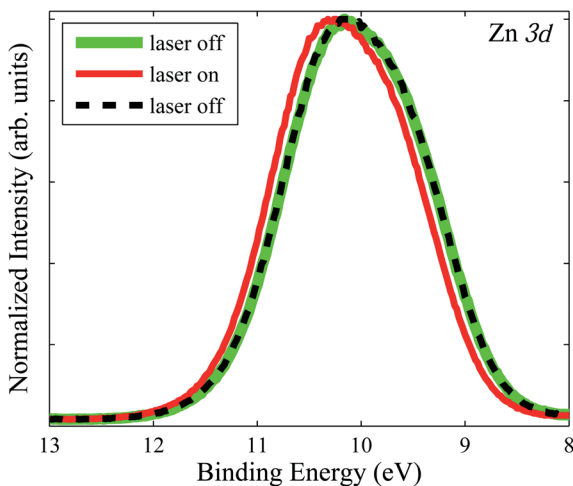


Fig. 7 The Zn 3*d* core level of the *m*-plane ZnO surface recorded using a photon energy of 200 eV with (red line) and without (green and dashed lines) laser photoexcitation with a CW laser (372 nm, 10 mW).



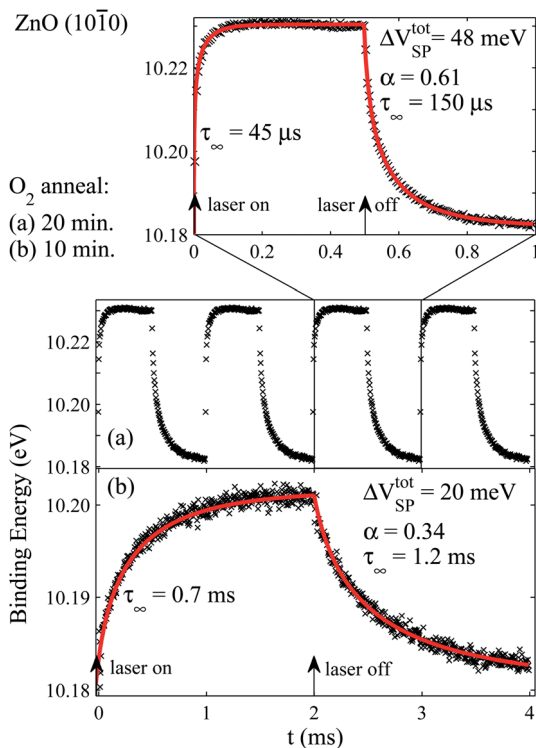


Fig. 8 Binding energy shift of the Zn  $3d$  core level of the ZnO  $m$ -plane surface recorded using a photon energy of 200 eV, during modulation of 3.33 eV (372 nm) CW illumination for a minimum of 10 000 data accumulations. Laser modulation is indicated by arrows. The samples were prepared identically (as described in the Experimental section) except for annealing in  $1.2\text{--}1.4 \times 10^{-7}$  mbar oxygen at 703 K for (a) 20 min and (b) 10 min (the experimental data in (a) are shown repeated on the time axis in the middle panel for comparison with (b)). The decay and onset of the pump-induced SPV are fitted using eqn (4) and an analogous decelerating exponential increase respectively (red lines). Reducing the oxygen annealing time from 20 min to 10 min leads to an increase in the dark carrier lifetime,  $\tau_{\infty}$ , of approximately one order of magnitude.

The change in the oxygen annealing treatment of the substrate changes the timescales of the SPV decay by approximately an order of magnitude, with the slowest SPV decay time found in the less oxygenated surface. We also note that this surface shows a smaller SPV shift; an SPV shift of 20 meV is measured in Fig. 8(b) (10 min oxygen anneal), compared with 48 meV in Fig. 8(a) (20 min oxygen anneal). The material parameter,  $\alpha$ , decreases from 0.61 to 0.34 as the oxygen annealing time is halved. The increase in  $\tau_{\infty}$  from a few hundred  $\mu\text{s}$  to around 1 ms on decreasing the oxygen annealing time in this way was found to be reproducible in several different experiments conducted on successive synchrotron beam runs.

In order to explore the possible role of oxygen-vacancy-related band-gap states in PPC,<sup>91</sup> separate experiments were also conducted using sub-band-gap excitation to excite a sample prepared in a similar way to that in Fig. 8(b), *i.e.* annealed in oxygen for 10 min. A pulsed laser of significantly sub-band-gap energy (wavelength 590 nm, or 2.10 eV) was used to illuminate the sample every 2 ms, at a delay



of 1 ms. No change in the position of the Zn  $3d$  peak was observed (Fig. 9); these laser pulses do not have enough energy to photoexcite electrons across the band gap of 3.4 eV, or to excite the broad 2.5 eV 'GD' (green defect) band.<sup>89</sup> However, a small photoresponse with a  $\tau_{\infty}$  of 570  $\mu\text{s}$  was measured following 405 nm (3.06 eV) excitation (Fig. 9). The observation of PPC using slightly sub-band-gap radiation is consistent with observations from ZnO nanowires.<sup>22,91,92</sup>

### ZnO (10 $\bar{1}0$ ) with chemically-linked PbS QDs

PbS QDs were chemically attached to the ZnO sample measured in Fig. 8(a) (prepared with a 20 min oxygen anneal). XPS shows the presence of the QDs at the surface. Fig. 10 shows the S  $2p$  core level XPS (analysed using CasaXPS<sup>93</sup>), where three species are identified as those associated with PbS (labelled S  $2p$  1),<sup>94</sup> neutral S (labelled S  $2p$  2)<sup>94</sup> and sulphur present in the 3-MPA ligand (labelled S  $2p$  3).<sup>95</sup> No oxidized species such as sulfite and sulfate (which are chemically shifted by  $\sim 4$  eV to higher BE)<sup>96,97</sup> were found,<sup>5</sup> suggesting the surfaces of the QDs are well passivated by the ligands.<sup>5</sup> The Pb  $4f$  core level is shown in Fig. 11, where two species are found associated with PbS (labelled PbS  $4f$  1) and Pb directly attached to the ligand (labelled PbS  $4f$  2).<sup>5,98</sup> An X-ray photon energy of 230 eV was used for both spectra (giving a sampling depth of approximately 1.5 nm). Fig. 11 shows that the ZnO substrate is sampled as well, as shown by the overlapping Zn  $3s$  signal.<sup>99</sup> All fits in Fig. 10 and 11 agree well with well-known literature parameters (doublet separations and BE positions), and these core levels were monitored to ensure laser damage was not occurring over the time period of the experiment. The valence band spectra for clean ZnO and with the PbS QDs attached are shown in Fig. 12, where the Zn  $3d$  core level signal is attenuated upon deposition of the QDs. Changes at the valence band energy ( $\sim 1$ –3 eV) are attributed to the QDs,<sup>5</sup> where the valence band maximum corresponds to the highest occupied molecular orbit (HOMO) of the QD, at a lower BE than the clean ZnO, consistent with the

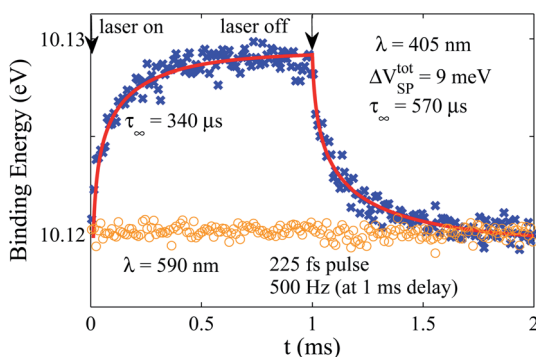


Fig. 9 Binding energy shift of the Zn  $3d$  core level of the ZnO  $m$ -plane surface recorded using a photon energy of 200 eV, during modulation of 3.06 eV (405 nm) CW laser illumination (blue crosses) for a minimum of 10 000 data accumulations. The sample was prepared as in Fig. 7(b). CW laser modulation is indicated by arrows. A dark carrier lifetime,  $\tau_{\infty}$ , of 570  $\mu\text{s}$  is obtained by fitting with the self-deceleration model of eqn (4). Also shown is the binding energy of the Zn  $3d$  core level during illumination with 590 nm (2.10 eV) radiation (orange circles). Here a pulsed laser (225 fs pulse width) was modulated at 500 Hz, *i.e.* every 2 ms, with a delay of 1 ms.



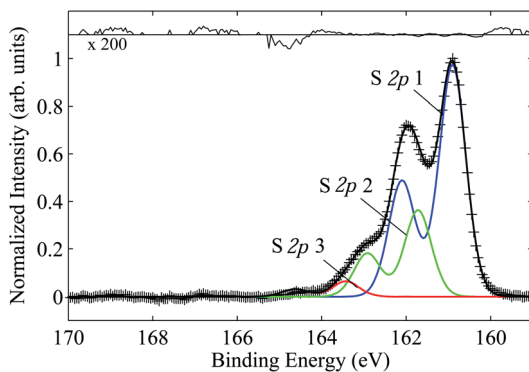


Fig. 10 XPS of the S  $2p$  core level measured using a photon energy of 230 eV. Three species are identified as being associated to PbS (1), neutral sulphur (2) and sulphur in the ligand (3). No features at higher BE due to oxidised species are observed. A magnified residual is shown above.

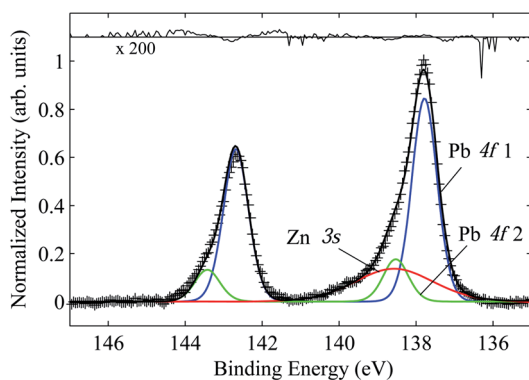


Fig. 11 XPS of the Pb  $4f$  core level measured using a photon energy of 230 eV. Two species are present which are due to PbS (1) and Pb atoms linked to the ligand (2). The Zn  $3s$  core level is also observed.

energy level line-up shown in Fig. 6(a). The increased signal in the BE range 4–8 eV after linking the QDs is due to the 3-MPA ligands.<sup>6</sup> A weak signal from the Pb  $5d$  core level is present at  $\sim 18.7$  eV with a doublet separation of  $\sim 2.5$  eV, consistent with literature values for PbS.<sup>94,100</sup>

The transient SPV measured with the Zn  $3d$  core level as in Fig. 8 was repeated, again using an exciting 372 nm laser. The ZnO sample was prepared and measured as shown in Fig. 8(a) (using a 20 min oxygen anneal) directly before the PbS QDs were linked to the surface. Fig. 13 shows that both the onset and decay times of the SPV decrease when QDs are attached to the surface. Indeed, the rising edge of the onset approaches the time resolution of the experiment ( $\sim 150$  ns), although the rise can be fitted with a rise time of 5  $\mu$ s. The dark carrier lifetime,  $\tau_{\infty}$ , decreases from 150  $\mu$ s to 65  $\mu$ s. The size of the SPV shift,  $\Delta V_{SP}^{tot}$ , also decreases from 48 meV to 15 meV and the material parameter,  $\alpha$ , is decreased to 0.16 compared to 0.61 for the clean case shown in Fig. 8(a).



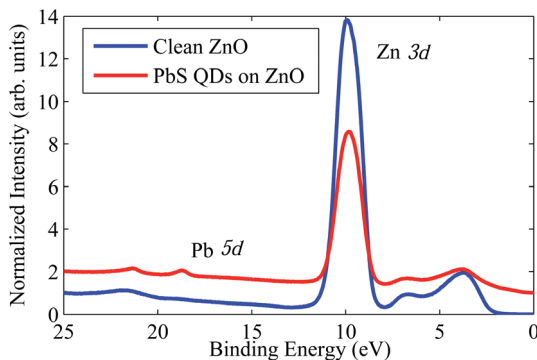


Fig. 12 XPS of the valence band of clean ZnO and PbS QDs attached to ZnO measured using a photon energy of 200 eV. The spectra have been normalized to the background at 25 eV BE and the PbS QDs spectrum has been offset vertically, showing changes in the valence band attributed to the QDs and 3-MPA ligands (see text). The Pb 5*d* core level is also observed at ~18.7 eV BE.

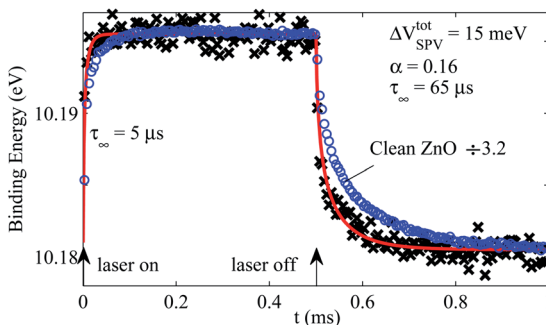


Fig. 13 Binding energy shift of the Zn 3*d* core level of the ZnO *m*-plane surface with PbS QDs chemically attached (black crosses), and of clean ZnO (blue circles, scaled down by a factor of 3.2 for comparison), recorded using a photon energy of 200 eV, during modulation of 3.33 eV (372 nm) CW illumination for a minimum of 10 000 data accumulations. Laser modulation is indicated by arrows. The decay and onset of the pump-induced SPV are fitted using eqn (4) and an analogous decelerating exponential increase respectively (red lines). The decay lifetime, SPV shift and material parameter,  $\alpha$ , are reduced when QDs are attached to the surface compared to the clean ZnO case (see text).

### ZnO (10 $\bar{1}$ 0) with chemically-linked CdS–ZnSe QDs

Type II CdS–ZnSe core–shell QDs were chemically attached to ZnO in the same way as the PbS QD sample. The ZnO surface was prepared using a 10 min anneal as in Fig. 8(b). Fig. 14 shows the Zn 3*p* XPS measured using a photon energy of 800 eV. Three doublets are required to fit the spectrum, with the main doublet associated with ZnO at 88.3 eV BE (labelled Zn 3*p* 1),<sup>99</sup> a weak component associated with ZnSe in the shell of the QD at 2.0 eV lower BE (labelled Zn 3*p* 2),<sup>101</sup> and a doublet at 1.9 eV higher BE associated with attachment to the ligand (labelled Zn 3*p* 3). Doublets were fitted with a spin orbit splitting of 3.0 eV.<sup>102</sup> The fact that there are now additional Zn photoemission lines associated with the QDs and the attaching ligands means that the transient SPV fitting of the Zn 3*d* core level



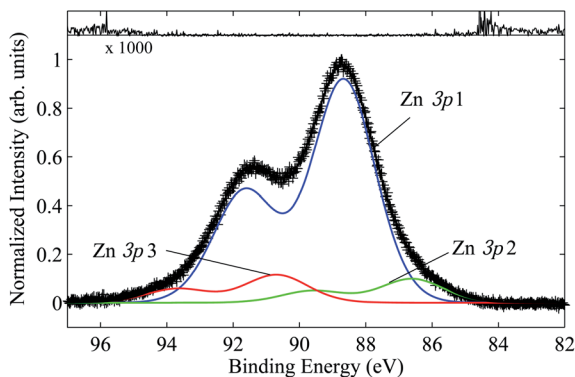


Fig. 14 Zn 3*p* XPS measured using a photon energy of 800 eV, showing three species associated with ZnO (1), ZnSe in the shell of the QD (2), and Zn linked to the ligand (3).

should involve fitting with more than one doublet. Fig. 15 shows the XPS of the Se 3*p* and S 2*p* core levels measured with a photon energy of 600 eV. There are two species of S, one associated with CdS (*S* 2*p*<sub>3/2</sub> at 161.7 eV BE) with a spin-orbit splitting of 1.2 eV (labelled *S* 2*p* 1),<sup>103</sup> and a species chemically shifted by 1.9 eV to higher BE associated with S in the 3-MPA ligand (labelled *S* 2*p* 2); the 'ligand' chemical shift is identical to that seen in the *S* 2*p* spectra of the PbS QDs shown in Fig. 10. The Se 3*p*<sub>3/2</sub> feature is present at 160.1 eV BE with a spin-orbit splitting of 5.6 eV,<sup>104</sup> and again all fitting parameters agree well with literature values. No oxidized S species in the range 168–172 eV BE are found. The Cd 3*d* core level was recorded at a BE position of 405 eV in agreement with literature values for CdS.<sup>103</sup>

Fig. 16 shows the valence band for the clean ZnO and with the CdS–ZnSe QDs attached. As for the PbS QD–ZnO system, there is a shift of the valence band edge to slightly lower BE on linking the QDs to the surface in agreement with the energy level line-up diagram in Fig. 6(b), there is a small amount of additional

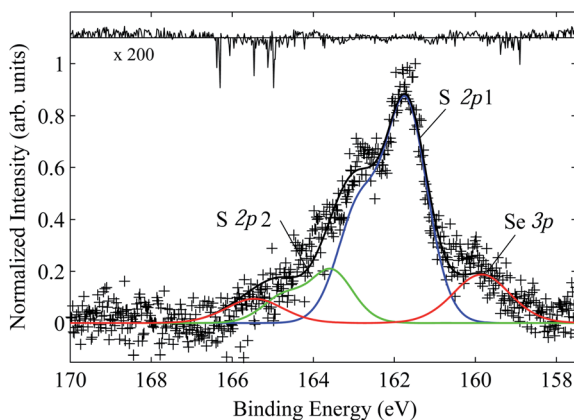


Fig. 15 XPS of the Se 3*p* and S 2*p* core levels measured with a photon energy of 600 eV. Two species of S 2*p* are identified as that associated with the CdS core of the QD (1) and sulfur in the 3-MPA ligand (2).



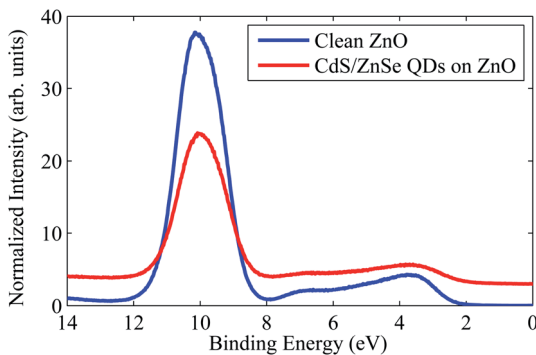


Fig. 16 Valence band XPS of clean ZnO and with CdS–ZnSe QDs chemically attached, measured using a photon energy of 200 eV. The spectra have been normalized to the background at 14 eV BE and the QD spectrum has been offset vertically to show changes in the valence band associated with the QDs and ligands (see text).

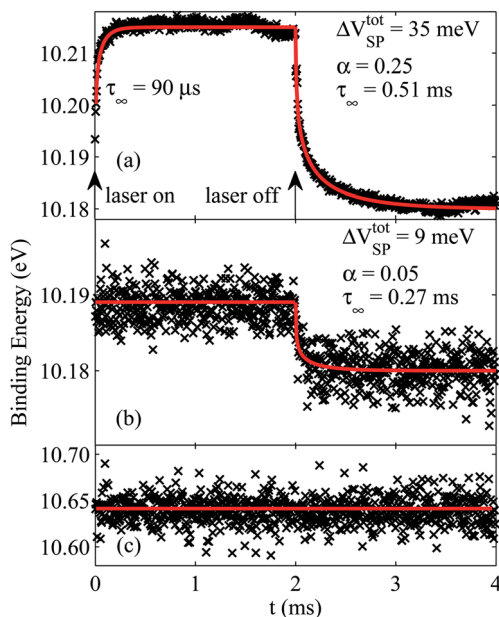


Fig. 17 Binding energy shift of the Zn 3d core level of (a) the ZnO *m*-plane surface, (b, c) the same surface with CdS–ZnSe QDs chemically attached, recorded using a photon energy of 200 eV, during modulation of 3.33 eV (372 nm) CW illumination for a minimum of 10 000 data accumulations. Laser modulation is indicated by arrows. The decay and onset of the pump-induced SPV are fitted using eqn (4) and an analogous decelerating exponential increase respectively (red lines). For the QD case where Zn is present in the shell, two components are fitted to the XPS spectra at each time interval. The lower BE component associated with the substrate (b) shows a reduced decay lifetime, SPV shift and material parameter,  $\alpha$ , when QDs are attached to the surface (see text). (c) shows the transient signal of the higher BE component associated with Zn attached to the ligand which does not change upon photoexcitation.



intensity between 4 and 8 eV BE associated with the ligand,<sup>6</sup> and the Zn 3*d* core level intensity is attenuated by the covering of QDs.

The transient SPV of the Zn 3*d* core level of the ZnO surface when illuminated with 372 nm (3.33 eV) laser radiation was measured before and after chemically linking the CdS–ZnSe QDs, as shown in Fig. 17(a) and 17(b), respectively. A photon energy of 200 eV was used. The clean ZnO surface shows a dark carrier lifetime of 0.51 ms and the fitted material parameter is 0.25, similar to that found for the surface measured in Fig. 8(b), which was annealed in oxygen for a similar time. XPS taken before and after the time-resolved measurements verified that there was no significant laser damage during the experiment.

When the QDs are attached to the surface, the dark carrier lifetime decreases (here to 0.27 ms) as found in the PbS QD sample. The initial rising edge of the onset now appears as a step function, suggesting that the dynamics are happening on faster timescales than the time resolution of the experiment. The material parameter also decreases, here to 0.05, and the SPV shift is reduced from 35 meV to 9 meV. The 3.33 eV laser is energetic enough to photoexcite carriers into the ZnSe shell, meaning these two QD samples can directly inject carriers into the ZnO conduction band upon photoexcitation. The Zn 3*d* core level for this experiment required two components to be fitted to the XPS. The fitted secondary doublet associated with the QD does not shift upon photoexcitation as shown in Fig. 17(c), as anticipated, as only the ZnO substrate is subject to a change in band bending on photoexcitation. The secondary component is fitted at approximately 0.5 eV higher BE than the doublet associated with the ZnO substrate, indicating this component is associated with Zn attached to the ligand. Only the onset of this higher BE component is fit due to the BE window available.

## Discussion

The change in the surface potential upon photoexcitation with 3.33 eV laser radiation has been observed for the *m*-plane ZnO (10 $\bar{1}$ 0) surface, first with different oxygen vacancy concentrations (adjusted by different durations of annealing in oxygen during surface preparation), and with two quantum dot samples, type I PbS and type II CdS–ZnSe core–shell QDs, chemically linked to the surface with 3-MPA ligands.

The decay in the ZnO SPV shift following photoexcitation occurs on relatively long timescales, typically over several ms here, which is a persistent photoconductivity (PPC). Rival explanations for the origin of this PPC all rely on the availability of oxygen. In the oxygen photodesorption model,<sup>8–14</sup> oxygen is provided by the environment by chemisorption at the surface, whereas in the model based on metastable band-gap defect states, the concentration of lattice oxygen vacancies controls the PPC.<sup>19,20,89–91</sup> The highly-controlled nature of our experiments under UHV conditions (where the residual vacuum was  $\sim 1.5 \times 10^{-10}$  mbar) allows for these two effects to be distinguished. Calculations of the initial oxygen vacancy concentration created by the 10 and 20 min O<sub>2</sub> annealing cycles and the estimated effect of these on the dynamics shown in Fig. 8 (a) and (b) lead us to conclude that the observed dynamics are at least  $10^3$ – $10^4$  times faster than can be explained by the oxygen photodesorption model.<sup>21</sup> The observation of PPC using sub-band gap photoexcitation (Fig. 9), allows us to demonstrate that an alternative model for PPC in ZnO (involving lattice oxygen vacancies) is dominant



in these experiments.<sup>21</sup> Our results show that defect states approximately 340 meV above the valence band edge are directly associated with the PPC, consistent with the hypothesis that ionized oxygen vacancy states are responsible for PPC in ZnO.<sup>18,21</sup> These results support similar measurements from ZnO nanowires.<sup>22,90,91</sup>

The onset of the SPV shown in Fig. 8 and 9 can be understood as a competition between the constant rate of photogeneration of carriers produced by the CW laser illumination and the recombination process, and as such the onset is expected to be faster than the decay times as observed throughout (Fig. 8, 9, 13 and 17). When the laser fluence is high, the onset of such SPV transients may be fitted using a single exponential that yields a time constant inversely proportional to the intensity of illumination.<sup>44</sup> However, fitting with a single exponential is not possible here, indicating the laser fluence is not sufficiently high for the optical generation to completely dominate the charge dynamics. Therefore, the onset of the SPV is instead fitted with a decelerated exponential model analogous to eqn (4), which reflects the dynamic increase in recombination rate as the surface band bending is reduced, which acts to counterbalance the rate of carrier photogeneration.

The 3.33 eV photoexcitation laser has sufficient energy to photoexcite electrons in both the PbS and the shell of the CdS–ZnSe QDs. In both cases, the effect of attachment of these QD samples to the surface of ZnO is to reduce the total change in the surface photovoltage,  $\Delta V_{SPV}^{tot}$ , reduce the material parameter,  $\alpha$ , and to reduce the dark carrier lifetime,  $\tau_{\infty}$ . The onset time of the SPV change was also reduced in both cases. Fig. 13 and 17 (b) show fast initial onsets, suggesting the dynamics here are occurring on timescales faster than the time resolution of the experiment (*ca.* 150 ns). This is anticipated if direct injection of charge from the QDs into the ZnO is occurring; charge injection from QDs into oxide surfaces may occur on fs timescales.<sup>105,106</sup>

Both samples were chemically attached with 3-MPA ligands. Valence band and core level XPS for both samples (Fig. 10–12, 14–16) show features associated with these ligands. The consistent decrease in the material parameter,  $\alpha$ , which has been shown to scale with the equilibrium band bending,<sup>61</sup> along with the consistent decrease in the total SPV change measured, suggests that the adsorbed QDs at the surface lead to a decrease in the equilibrium band bending at the ZnO surface, through charge donation into the depletion layer at the surface of *n*-type ZnO. This decrease in the surface potential causes the photoexcited carrier lifetimes to change (according to eqn (2)), as well as the total SPV change measured upon photoexcitation (eqn (1)). Therefore, the data suggest that photoexcited carriers in the PbS QDs and in the shell of the CdS–ZnSe QDs are injected into the conduction band of the ZnO substrate instantaneously (relative to the intrinsic time resolution of the experiment), causing the band bending to immediately be reduced (observed as a shift to higher BE of the Zn 3*d* core level). In the clean ZnO samples the onset can be understood to be due to photogeneration by the CW laser competing with the lifetime of the generated carriers, whereas upon deposition of the QDs, a new, faster route for photoinjection into the ZnO conduction band from the QDs is opened up. This fast injection of carriers from QD to substrate is consistent with the energy level line-up diagrams illustrated in Fig. 6(a) and (b), and with other literature investigating charge transfer in similar systems involving QDs chemically linked to TCOs,<sup>107–113</sup> which may be occurring on ps and fs timescales.<sup>105,106,114</sup>



The results presented here suggest the need for further experimentation into charge transfer between quantum dots and transparent conducting oxide substrates. Photoexcitation of the systems with laser photon energies greater than the effective band gap of the QDs, but insufficient energy to directly photoexcite the substrate is a logical next step. A transient SPV in the substrate when only the QDs have been photoexcited would confirm that carriers have been injected from the QD into the substrate.

There is also a clear need for laser pump-X-ray probe methodologies that allow for relatively long timescales to be measured (*e.g.* ms as required to measure the transient SPV for PPC in ZnO) with a much greater timing resolution (on sub ps timescales) in order to effectively resolve ultrafast onsets of transient SPV once QDs are attached to the surface. Clearly, the advent of 4<sup>th</sup> generation radiation from FELs and other low emittance electron beam sources, combined with time-of-flight electron energy analysis,<sup>54</sup> provides a route to addressing this issue, provided sample damage can be controlled.

These results demonstrate the potential for light-harvesting quantum dots attached to ZnO as a basis for next-generation solar cells. As the effective band gap energy of QDs can be tuned by varying the QD diameter, these light harvesters can be optimized to absorb the majority of the solar energy spectrum, and the use of type II QDs allows recombination rates to be reduced. The lifetime of carriers injected into the ZnO conduction band is by comparison very long, and can be tuned by varying the oxygen vacancy concentration in the sample, controlled by the preparation process. Thus charge can be extracted from the system efficiently before significant recombination has occurred.

## Conclusions

Photoexcited carrier dynamics have been investigated in the potential next-generation photoanode material ZnO (using the nonpolar *m*-plane (10 $\bar{1}$ 0) surface). A laser pump-X-ray probe methodology has allowed for the transient change in the surface potential upon photoexcitation to be measured. PPC is observed in ZnO where recombination of carriers occurs on ms timescales. The highly-controlled nature of the experiment under UHV, as well as photoexcitation with sub-band gap radiation, has allowed us to show that this PPC originates from defect band-gap states (340 meV above the valence band maximum) associated with lattice oxygen vacancies.<sup>18,21</sup> Light-harvesting colloidal quantum dots have been chemically linked to the surface with 3-MPA ligands. The total change in the surface photovoltage, the material parameter,  $\alpha$ , and dark carrier lifetime consistently decrease when PbS and type II CdS–ZnSe core–shell QDs are attached to the ZnO surface. These changes are likely to be due to a decrease in the equilibrium band bending at the surface due to charge donation from the QD into the depletion layer at the surface of *n*-type ZnO. The initial onset times for the transient SPV are also decreased, suggesting that the onset of the SPV is occurring within the time resolution of the experiments. This suggests that direct injection of charge carriers from the QD into the conduction band of the substrate is occurring. The combination of fast electron injection with a very slow recombination rate due to PPC in the ZnO photoanode means that the system therefore shows great potential in next-generation solar cell technology.



Laser pump-X-ray probe measurements are powerful probes of photoexcited carrier dynamics over a wide range of timescales. The results presented here indicate a need for further studies in this area, and for development of methodologies capable of measuring relatively long (ms) timescales with increased (sub-ps) timing resolution.

## Acknowledgements

The research leading to these results received funding from the European Community's Seventh Framework Programme (FP7/2007-2013) under grant agreement no 226716, allowing access to Synchrotron SOLEIL. Work was also supported by the Cockcroft Institute *via* its STFC core grant ST/G008248/1.

## Notes and references

- 1 P. D. C. King and T. D. Veal, *J. Phys.: Condens. Matter*, 2011, **23**, 334214.
- 2 C. F. Klingshirn, *Zinc Oxide: from fundamental properties towards novel applications*, Springer, Heidelberg; London, 2010.
- 3 C. Klingshirn, J. Fallert, H. Zhou, J. Sartor, C. Thiele, F. Maier-Flaig, D. Schneider and H. Kalt, *Phys. Status Solidi B*, 2010, **247**, 1424.
- 4 B. Carlson, K. Leschkies, E. S. Aydil and X. Y. Zhu, *J. Phys. Chem. C*, 2008, **112**, 8419.
- 5 S. J. O. Hardman, D. M. Graham, S. K. Stubbs, B. F. Spencer, E. A. Seddon, H. T. Fung, S. Gardonio, F. Sirotti, M. G. Silly, J. Akhtar, P. O'Brien, D. J. Binks and W. R. Flavell, *Phys. Chem. Chem. Phys.*, 2011, **13**, 20275.
- 6 J. Akhtar, M. A. Malik, P. O'Brien, K. G. U. Wijayantha, R. Dharmadasa, S. J. O. Hardman, D. M. Graham, B. F. Spencer, S. K. Stubbs, W. R. Flavell, D. J. Binks, F. Sirotti, M. El Kazzi and M. Silly, *J. Mater. Chem.*, 2010, **20**, 2336.
- 7 J. A. McLeod, R. G. Wilks, N. A. Skorikov, L. D. Finkelstein, M. Abu-Samak, E. Z. Kurmaev and A. Moewes, *Phys. Rev. B: Condens. Matter Mater. Phys.*, 2010, **81**, 245123.
- 8 I. Tashiro, T. Kimura and K. Endo, *Appl. Opt.*, 1969, **8**, 180.
- 9 J. Lagowski, E. S. Sproles and H. C. Gatos, *J. Appl. Phys.*, 1977, **48**, 3566.
- 10 A. Rothschild, Y. Komem and N. Ashkenasy, *J. Appl. Phys.*, 2002, **92**, 7090.
- 11 X. G. Zheng, Q. S. Li, W. Hu, D. Chen, N. Zhang, M. J. Shi, J. J. Wang and L. C. Zhang, *J. Lumin.*, 2007, **122**, 198.
- 12 T. E. Murphy, K. Moazzami and J. D. Phillips, *J. Electron. Mater.*, 2006, **35**, 543.
- 13 R. J. Collins and D. G. Thomas, *Phys. Rev.*, 1958, **112**, 388.
- 14 M. J. Liu and H. K. Kim, *Appl. Phys. Lett.*, 2004, **84**, 173.
- 15 D. C. Hou, A. Dev, K. Frank, A. Rosenauer and T. Voss, *J. Phys. Chem. C*, 2012, **116**, 19604.
- 16 J. M. Bao, I. Shalish, Z. H. Su, R. Gurwitz, F. Capasso, X. W. Wang and Z. F. Ren, *Nanoscale Res. Lett.*, 2011, **6**, 404.
- 17 S. Lany and A. Zunger, *Phys. Rev. Lett.*, 2007, **98**, 045501.
- 18 S. Lany and A. Zunger, *Phys. Rev. B: Condens. Matter Mater. Phys.*, 2005, **72**, 035215.
- 19 S. B. Zhang, S. H. Wei and A. Zunger, *Phys. Rev. B: Condens. Matter*, 2001, **63**, 075205.
- 20 A. Janotti and C. G. Van de Walle, *Appl. Phys. Lett.*, 2005, **87**, 122102.



- 21 B. F. Spencer, D. M. Graham, S. J. O. Hardman, E. A. Seddon, M. J. Cliffe, K. L. Syres, A. G. Thomas, S. K. Stubbs, F. Sirotti, M. G. Silly, P. F. Kirkham, A. R. Kumarasinghe, G. J. Hirst, A. J. Moss, S. F. Hill, D. A. Shaw, S. Chattopadhyay and W. R. Flavell, *Phys. Rev. B: Condens. Matter Mater. Phys.*, 2013, **88**, 195301.
- 22 I. Beinik, M. Kratzer, A. Wachauer, L. Wang, Y. P. Piryatinski, G. Brauer, X. Y. Chen, Y. F. Hsu, A. B. Djuricic and C. Teichert, *Beilstein J. Nanotechnol.*, 2013, **4**, 208.
- 23 V. I. Klimov, *Semiconductor and metal nanocrystals: synthesis and electronic and optical properties*, Marcel Dekker, New York, 2004.
- 24 V. I. Klimov, *Nanocrystal quantum dots*, 2nd edn, CRC Press, Boca Raton, 2010.
- 25 R. D. Schaller and V. I. Klimov, *Abstr Pap Am Chem S*, 2005, **229**, U729.
- 26 R. D. Schaller and V. I. Klimov, *Phys. Rev. Lett.*, 2004, **92**, 186601.
- 27 R. D. Schaller, M. Sykora, S. Jeong and V. I. Klimov, *J. Phys. Chem. B*, 2006, **110**, 25332.
- 28 W. Shockley and H. J. Queisser, *J. Appl. Phys.*, 1961, **32**, 510.
- 29 S. K. Stubbs, S. J. O. Hardman, D. M. Graham, B. F. Spencer, W. R. Flavell, P. Glarvey, O. Masala, N. L. Pickett and D. J. Binks, *Phys. Rev. B: Condens. Matter Mater. Phys.*, 2010, **81**, 081303(R).
- 30 R. D. Schaller, J. M. Pietryga and V. I. Klimov, *Nano Lett.*, 2007, **7**, 3469.
- 31 R. D. Schaller, M. A. Petruska and V. I. Klimov, *Appl. Phys. Lett.*, 2005, **87**, 253102.
- 32 Y. Kobayashi, T. Udagawa and N. Tamai, *Chem. Lett.*, 2009, **38**, 830.
- 33 M. C. Beard, K. P. Knutsen, P. R. Yu, J. M. Luther, Q. Song, W. K. Metzger, R. J. Ellingson and A. J. Nozik, *Nano Lett.*, 2007, **7**, 2506.
- 34 J. B. Sambur, T. Novet and B. A. Parkinson, *Science*, 2010, **330**, 63.
- 35 V. I. Klimov, S. A. Ivanov, J. Nanda, M. Achermann, I. Bezel, J. A. McGuire and A. Piryatinski, *Nature*, 2007, **447**, 441.
- 36 A. Piryatinski, S. A. Ivanov, S. Tretiak and V. I. Klimov, *Nano Lett.*, 2007, **7**, 108.
- 37 S. Kim, B. Fisher, H. J. Eisler and M. Bawendi, *J. Am. Chem. Soc.*, 2003, **125**, 11466.
- 38 S. Kaniyankandy, S. Rawalekar, S. Verma and H. N. Ghosh, *J. Phys. Chem. C*, 2011, **115**, 1428.
- 39 S. Rawalekar, S. Kaniyankandy, S. Verma and H. N. Ghosh, *J. Phys. Chem. C*, 2010, **114**, 1460.
- 40 S. Rawalekar, S. Kaniyankandy, S. Verma and H. N. Ghosh, *J. Phys. Chem. C*, 2011, **115**, 12335.
- 41 D. Oron, M. Kazes and U. Banin, *Phys. Rev. B: Condens. Matter Mater. Phys.*, 2007, **75**, 035330.
- 42 S. M. Fairclough, E. J. Tyrrell, D. M. Graham, P. J. B. Lunt, S. J. O. Hardman, A. Pietzsch, F. Hennies, J. Moghal, W. R. Flavell, A. A. R. Watt and J. M. Smith, *J. Phys. Chem. C*, 2012, **116**, 26898.
- 43 M. Cadirci, S. K. Stubbs, S. M. Fairclough, E. J. Tyrrell, A. A. R. Watt, J. M. Smith and D. J. Binks, *Phys. Chem. Chem. Phys.*, 2012, **14**, 13638.
- 44 L. Kronik and Y. Shapira, *Surf. Sci. Rep.*, 1999, **37**, 1.
- 45 M. H. Hecht, *Phys. Rev. B: Condens. Matter*, 1991, **43**, 12102.
- 46 J. P. Long, H. R. Sadeghi, J. C. Rife and M. N. Kabler, *Phys. Rev. Lett.*, 1990, **64**, 1158.



- 47 S. Tanaka, S. D. More, J. Murakami, M. Itoh, Y. Fujii and M. Kamada, *Phys. Rev. B: Condens. Matter*, 2001, **64**, 155308.
- 48 S. Tanaka, T. Nishitani, T. Nakanishi, S. D. More, J. Azuma, K. Takahashi, O. Watanabe and M. Kamada, *J. Appl. Phys.*, 2004, **95**, 551.
- 49 S. Tanaka, T. Ichibayashi and K. Tanimura, *Phys. Rev. B: Condens. Matter Mater. Phys.*, 2009, **79**, 155313.
- 50 W. Widdra, D. Bröcker, T. Gießel, I. V. Hertel, W. Kruger, A. Liero, F. Noack, V. Petrov, D. Pop, P. M. Schmidt, R. Weber, I. Will and B. Winter, *Surf. Sci.*, 2003, **543**, 87.
- 51 D. Bröcker, T. Gießel and W. Widdra, *Chem. Phys.*, 2004, **299**, 247.
- 52 T. E. Glover, G. D. Ackermann, A. Belkacem, B. Feinberg, P. A. Heimann, Z. Hussain, H. A. Padmore, C. Ray, R. W. Schoenlein and W. F. Steele, *Nucl. Instrum. Methods Phys. Res., Sect. A*, 2001, **467**, 1438.
- 53 T. E. Glover, G. D. Ackermann, Z. Hussain and H. A. Padmore, *J. Mod. Opt.*, 2004, **51**, 2805.
- 54 M. Ogawa, S. Yamamoto, Y. Kousa, F. Nakamura, R. Yukawa, A. Fukushima, A. Harasawa, H. Kondoh, Y. Tanaka, A. Kakizaki and I. Matsuda, *Rev. Sci. Instrum.*, 2012, **83**, 023109.
- 55 A. Vollmer, R. Ovsyannikov, M. Gorgoi, S. Krause, M. Oehzelt, A. Lindblad, N. Martensson, S. Svensson, P. Karlsson, M. Lundvuis, T. Schmeiler, J. Pflaum and N. Koch, *J. Electron Spectrosc. Relat. Phenom.*, 2012, **185**, 55.
- 56 M. Hajlaoui, E. Papalazarou, J. Mauchain, G. Lantz, N. Moisan, D. Boschetto, Z. Jiang, I. Miotkowski, Y. P. Chen, A. Taleb-Ibrahimi, L. Perfetti and M. Marsi, *Nano Lett.*, 2012, **12**, 3532.
- 57 M. Marsi, M. E. Couprie, L. Nahon, D. Garzella, T. Hara, R. Bakker, M. Billardon, A. Delboulbe, G. Indlekofer and A. Taleb-Ibrahimi, *Appl. Phys. Lett.*, 1997, **70**, 895.
- 58 M. Marsi, R. Belkhou, C. Grupp, G. Panaccione, A. Taleb-Ibrahimi, L. Nahon, D. Garzella, D. Nutarelli, E. Renault, R. Roux, M. E. Couprie and M. Billardon, *Phys. Rev. B: Condens. Matter*, 2000, **61**, R5070.
- 59 S. Yamamoto and I. Matsuda, *J Phys Soc Jpn*, 2013, **82**, 00213.
- 60 J. P. Long and V. M. Bermudez, *Phys. Rev. B: Condens. Matter*, 2002, **66**, 121308.
- 61 J. Schulz, P. Wurfel and W. Ruppel, *Phys. Status Solidi B*, 1991, **164**, 425.
- 62 F. Polack, M. Silly, C. Chauvet, B. Lagarde, N. Bergéard, M. Izquierdo, O. Chubar, D. Krizmancic, M. Ribbens, J. P. Duval, C. Basset, S. Kubsky and F. Sirotti, *AIP proceedings: The 10th International Conference on Synchrotron Radiation Instrumentation*, 2010, **1234**, 185.
- 63 N. Bergéard, M. G. Silly, D. Krizmancic, C. Chauvet, M. Guzzo, J. P. Ricaud, M. Izquierdo, L. Stebel, P. Pittana, R. Sergo, G. Cautero, G. Dufour, F. Rochet and F. Sirotti, *J. Synchrotron Radiat.*, 2011, **18**, 245.
- 64 G. Cautero, R. Sergo, L. Stebel, P. Lacovig, P. Pittana, M. Predonzani and S. Carrato, *Nucl. Instrum. Methods Phys. Res., Sect. A*, 2008, **595**, 447.
- 65 K. Ozawa and K. Edamoto, *Surf. Sci.*, 2003, **524**, 78.
- 66 W. Göpel and U. Lampe, *Phys. Rev. B*, 1980, **22**, 6447.
- 67 W. Göpel, *Surf. Sci.*, 1977, **62**, 165.
- 68 O. Dulub, L. A. Boatner and U. Diebold, *Surf. Sci.*, 2002, **519**, 201.
- 69 U. Diebold, L. V. Koplitz and O. Dulub, *Appl. Surf. Sci.*, 2004, **237**, 336.



- 70 S. J. Pearton, D. P. Norton, K. Ip, Y. W. Heo and T. Steiner, *Prog. Mater. Sci.*, 2005, **50**, 293.
- 71 J. M. Lee, K. K. Kim, S. J. Park and W. K. Choi, *Appl. Phys. Lett.*, 2001, **78**, 3842.
- 72 V. E. Henrich and P. A. Cox, *The surface science of metal oxides*, Cambridge University Press, Cambridge; New York, 1994.
- 73 G. W. Tomlins, J. L. Routbort and T. O. Mason, *J. Am. Ceram. Soc.*, 1998, **81**, 869.
- 74 A. C. S. Sabioni, A. M. J. M. Daniel, W. B. Ferraz, R. W. D. Pais, A. M. Huntz and F. Jomard, *Mater Res-Ibero-Am J*, 2008, **11**, 221.
- 75 I. S. Jeong, J. H. Kim and S. Im, *Appl. Phys. Lett.*, 2003, **83**, 2946.
- 76 W. A. Tisdale, M. Muntwiler, D. J. Norris, E. S. Aydil and X. Y. Zhu, *J. Phys. Chem. C*, 2008, **112**, 14682.
- 77 L. Cademartiri, E. Montanari, G. Calestani, A. Migliori, A. Guagliardi and G. A. Ozin, *J. Am. Chem. Soc.*, 2006, **128**, 10337.
- 78 X. H. Zhong, Y. Y. Feng and Y. L. Zhang, *J. Phys. Chem. C*, 2007, **111**, 526.
- 79 B. Blackman, D. Battaglia and X. G. Peng, *Chem. Mater.*, 2008, **20**, 4847.
- 80 J. Bang, J. Park, J. H. Lee, N. Won, J. Nam, J. Lim, B. Y. Chang, H. J. Lee, B. Chon, J. Shin, J. B. Park, J. H. Choi, K. Cho, S. M. Park, T. Joo and S. Kim, *Chem. Mater.*, 2010, **22**, 233.
- 81 P. T. K. Chin, C. D. M. Donega, S. S. Bavel, S. C. J. Meskers, N. A. J. M. Sommerdijk and R. A. J. Janssen, *J. Am. Chem. Soc.*, 2007, **129**, 14880.
- 82 J. I. Kim, J. Kim, J. Lee, D. R. Jung, H. Kim, H. Choi, S. Lee, S. Byun, S. Kang and B. Park, *Nanoscale Res. Lett.*, 2012, **7**, 1.
- 83 X. Y. Wang, L. H. Qu, J. Y. Zhang, X. G. Peng and M. Xiao, *Nano Lett.*, 2003, **3**, 1103.
- 84 J. Aldana, Y. A. Wang and X. G. Peng, *J. Am. Chem. Soc.*, 2001, **123**, 8844.
- 85 M. W. Wang, J. O. Mccaldin, J. F. Swenberg, T. C. McGill and R. J. Hauenstein, *Appl. Phys. Lett.*, 1995, **66**, 1974.
- 86 S. A. Ivanov and M. Achermann, *ACS Nano*, 2010, **4**, 5994.
- 87 P. D. C. King, T. D. Veal, A. Schleife, J. Zuniga-Perez, B. Martel, P. H. Jefferson, F. Fuchs, V. Munoz-Sanjose, F. Bechstedt and C. F. McConville, *Phys. Rev. B: Condens. Matter Mater. Phys.*, 2009, **79**, 205205.
- 88 W. Göpel, J. Pollmann, I. Ivanov and B. Reihl, *Phys. Rev. B*, 1982, **26**, 3144.
- 89 H. L. Mosbacker, Y. M. Strzhemechny, B. D. White, P. E. Smith, D. C. Look, D. C. Reynolds, C. W. Litton and L. J. Brillson, *Appl. Phys. Lett.*, 2005, **87**, 012102.
- 90 A. Kushwaha and M. Aslam, *J. Appl. Phys.*, 2012, **112**, 054316.
- 91 P. Liu, G. W. She, Z. L. Liao, Y. Wang, Z. Z. Wang, W. S. Shi, X. H. Zhang, S. T. Lee and D. M. Chen, *Appl. Phys. Lett.*, 2009, **94**, 063120.
- 92 K. Keem, H. Kim, G. T. Kim, J. S. Lee, B. Min, K. Cho, M. Y. Sung and S. Kim, *Appl. Phys. Lett.*, 2004, **84**, 4376.
- 93 Casa XPS, [www.casaxps.com](http://www.casaxps.com).
- 94 R. B. Shalvoy, G. B. Fisher and P. J. Stiles, *Phys. Rev. B: Solid State*, 1977, **15**, 1680.
- 95 G. Gonella, O. Cavalleri, S. Terreni, D. Cvetko, L. Floreano, A. Morgante, M. Canepa and R. Rolandi, *Surf. Sci.*, 2004, **566**, 638.
- 96 B. J. Lindberg, *Acta Chem. Scand.*, 1970, **24**, 2242.
- 97 V. I. Nefedov, *Surf. Interface Anal.*, 1981, **3**, 72.



- 98 A. Lobo, T. Moller, M. Nagel, H. Borchert, S. G. Hickey and H. Weller, *J. Phys. Chem. B*, 2005, **109**, 17422.
- 99 B. R. Strohmeier and D. M. Hercules, *J. Catal.*, 1984, **86**, 266.
- 100 F. R. McFeely, S. Kowalczy, L. Ley, R. A. Pollak and D. A. Shirley, *Phys. Rev. B: Solid State*, 1973, **7**, 5228.
- 101 F. Y. Yang, D. Y. Ban, R. C. Fang, S. H. Xu, P. S. Xu and S. X. Yuan, *J. Electron Spectrosc. Relat. Phenom.*, 1996, **80**, 193.
- 102 A. Lebugle, U. Axelsson, R. Nyholm and N. Martensson, *Phys. Scr.*, 1981, **23**, 825.
- 103 E. Agostinelli, C. Battistoni, D. Fiorani and G. Mattogno, *J. Phys. Chem. Solids*, 1989, **50**, 269.
- 104 D. W. Langer and C. J. Vesely, *Phys. Rev. B: Solid State*, 1970, **2**, 4885.
- 105 W. A. Tisdale, K. J. Williams, B. A. Timp, D. J. Norris, E. S. Aydil and X. Y. Zhu, *Science*, 2010, **328**, 1543.
- 106 Y. Yang, W. Rodriguez-Cordoba, X. Xiang and T. Q. Lian, *Nano Lett.*, 2012, **12**, 303.
- 107 V. Gonzalez-Pedro, Q. Shen, V. Jovanovski, S. Gimenez, R. Tena-Zaera, T. Toyoda and I. Mora-Sero, *Electrochim. Acta*, 2013, **100**, 35.
- 108 A. G. Pattantyus-Abraham, I. J. Kramer, A. R. Barkhouse, X. H. Wang, G. Konstantatos, R. Debnath, L. Levina, I. Raabe, M. K. Nazeeruddin, M. Gratzel and E. H. Sargent, *ACS Nano*, 2010, **4**, 3374.
- 109 I. Robel, V. Subramanian, M. Kuno and P. V. Kamat, *J. Am. Chem. Soc.*, 2006, **128**, 2385.
- 110 K. S. Leschkies, R. Divakar, J. Basu, E. Enache-Pommer, J. E. Boercker, C. B. Carter, U. R. Kortshagen, D. J. Norris and E. S. Aydil, *Nano Lett.*, 2007, **7**, 1793.
- 111 B. R. Hyun, Y. W. Zhong, A. C. Bartnik, L. F. Sun, H. D. Abruna, F. W. Wise, J. D. Goodreau, J. R. Matthews, T. M. Leslie and N. F. Borrelli, *ACS Nano*, 2008, **2**, 2206.
- 112 D. F. Watson, *J. Phys. Chem. Lett.*, 2010, **1**, 2299.
- 113 X. W. Sun, J. Chen, J. L. Song, D. W. Zhao, W. Q. Deng and W. Lei, *Opt. Express*, 2010, **18**, 1296.
- 114 K. Zidek, K. B. Zheng, C. S. Ponseca, M. E. Messing, L. R. Wallenberg, P. Chabera, M. Abdellah, V. Sundstrom and T. Pullerits, *J. Am. Chem. Soc.*, 2012, **134**, 12110.

